

# Sun-Avoidance Slew Planning with Keep-Out Cone and Actuator Constraints

Mohammad A. Ayoubi \*

*Santa Clara University, 500 El Camino Real, Santa Clara, CA 95053*

Junette Hsin<sup>†</sup>

*Maxar Space Infrastructure (formerly Space Systems/Loral), 3825 Fabian Way, Palo Alto, CA 94303*

**This paper presents a geometric approach for a Sun (or any bright object) avoidance slew maneuver with pointing and actuator constraints. We assume that a gyrostat has a single light-sensitive payload with control-torque and reaction wheels' angular momentum constraints. Furthermore, we assume that the initial and final attitudes, an instrument's line-of-sight (LOS) vector, and sun vector are known. Then we use Pontryagin's minimum principle (PMP) and derive the desired or target-frame quaternions, angular velocity and acceleration. In the end, a Monte Carlo simulation is performed to show the viability of the proposed algorithm with control-torque and angular momentum constraints.**

## Nomenclature

$\hat{e}$	= unit vector along eigenaxis
$h$	= the total angular momentum of reaction wheel with respect to its center-of-mass
$I$	= the mass-moment-of-inertia of the gyrostat
$\hat{P}$	= unit position vector
$q$	= quaternion of one frame with respect to the other frame
$\mathbb{R}$	= set of real numbers
$\hat{S}$	= unit sun vector
$\mathcal{U}$	= set of all admissible controls
$\epsilon$	= instrument half-cone angle
$\alpha$	= the angle between the sun vector and the slew plane
$\omega$	= angular velocity of gyrostat

Subscripts or superscripts

$f$  = final state

\*Associate Professor, Department of Mechanical Engineering, Santa Clara University, 500 El Camino Real, Santa Clara, CA 95053, AIAA Senior Member.

<sup>†</sup>Engineer, Dynamics and Control Analysis Group, Maxar Space Infrastructure (formerly Space Systems/Loral), 3825 Fabian Way, Palo Alto, CA 94303.

$i$	=	initial state
$\mathcal{G}$	=	gyrostat body-fixed frame
$\mathcal{G}^*$	=	gyrostat's center-of-mass
$\mathcal{N}$	=	the Newtonian frame
$p$	=	payload
$T$	=	transpose of a matrix
$\mathcal{T}$	=	the target frame
$\mathcal{W}_i$	=	the $i^{th}$ reaction wheel frame
$\mathcal{W}_i^*$	=	center of mass of the $i^{th}$ reaction wheel

## I. Introduction

**L**ARGE-angle slew maneuvers are required during any Earth-pointing or interplanetary missions. In many space missions, and for safety considerations, a sensitive payload such as an imaging camera or telescope needs to be retargeted while avoiding the sun vector or other bright objects in the sky.

The attitude reorientation problem in the presence of attitude constrained zones has been studied in the last three decades. McInnes[1] addressed this problem via an artificial potential function. He proposed an entirely analytical guidance law which was suitable for onboard implementation. However, he used Euler angles, which are singular for large slew angles. A geometric approach was proposed by Spindle[2], Hablani[3], and Biggs and Colley[4] where a feasible attitude maneuver, or a guidance law, is precomputed based on the attitude-avoidance-zone constraints. Another approach for addressing this problem used randomized algorithms[5]. However, depending on the number of constraints and initial and final attitudes, this approach can be computationally expensive and not suitable for onboard implementation. Spiller et al.[6] proposed a method for solving the time optimal reorientation maneuver subject to boundaries and path constraints. They used the particle swarm optimization (PSO) technique to find a sub-optimal solution with keep-out constraints. Another approach casted the problem as a convex optimization problem and used semi-definite programming (SDP) or quadratically constrained quadratic programming (QCQP) in its solution (see for instance Kim and Mesbahi[7], Kim et al.[8], Sun and Dai[9], and Lee and Mesbahi[10]). Recently, Ramos and Schaub[11] proposed a method based on the Lyapunov stability theorem and logarithmic barrier potential function to derive a steering law for attitude control of a gyrostat subject to conically constrained inclusion and exclusion regions. They also considered the control-torque constraint in their algorithm.

In this paper, we present a novel geometric approach for large-angle slew planning with pointing and actuator constraints. We assume that the gyrostat has a single light-sensitive payload with control-torque and reaction wheels' angular momentum constraints. Furthermore, we assume that the initial and final attitudes, instrument's LOS vector, and

sun vector are known. Then, we derive the desired or target-frame quaternion, angular rate, and angular acceleration based on the Pontryagin's minimum principle (PMP) for the minimum-time, large slew angles. The precomputed target-frame quaternion is non-singular for large slew angles compared to Euler angle representation. The proposed method in this paper is time optimal, intuitive, deterministic, easy to implement, and includes the control-torque and reaction wheels' angular momentum constraints. The main drawback of the proposed algorithm is its limitation for a single sensitive-payload. A Monte Carlo simulation is performed to show the viability of the proposed algorithm with control-torque and angular momentum constraints.

## II. Problem Formulation

Consider a gyrostat, (a rigid body with reaction wheels) and let us define a Newtonian frame,  $N$ , and a gyrostat-centered unit sphere frame  $G$  with a center  $G^*$  as shown in Fig. 1. The sun or bright-object avoidance planning problem can be stated as follows:

Assume the initial state,  $x(t_i) = [\mathcal{N}\hat{P}_i, \mathcal{N}\omega^G(t_i), \mathcal{N}q^G(t_i)] \in \mathbb{R}^3 \times \mathbb{R}^3 \times \text{SO}(3)$ , final state,  $x(t_f) = [\mathcal{N}\hat{P}_f, \mathcal{N}\omega^G(t_f), \mathcal{N}q^G(t_f)] \in \mathbb{R}^3 \times \mathbb{R}^3 \times \text{SO}(3)$ , the sun unit vector in the  $N$ -frame,  $\mathcal{N}\hat{S} \in \mathbb{R}^3$ , the sensitive instrument's LOS unit vector in the  $G$ -frame,  $\mathcal{G}\hat{P} \in \mathbb{R}^3$ , and the half-cone angle  $\epsilon_p \in \mathbb{R}$  are given. The angular velocity of  $G$ -frame in  $N$ -frame, expressed in the  $G$ -frame denotes by  $\mathcal{N}\omega^G$  and the orientation of  $G$ -frame in  $N$ -frame denotes by  $\mathcal{N}q^G$ . Find a sequence of slew maneuvers such that the sun vector does not enter into the on-board sensitive instrument forbidden cone for all times  $t \in [t_i, t_f]$  subject to actuator constraints.

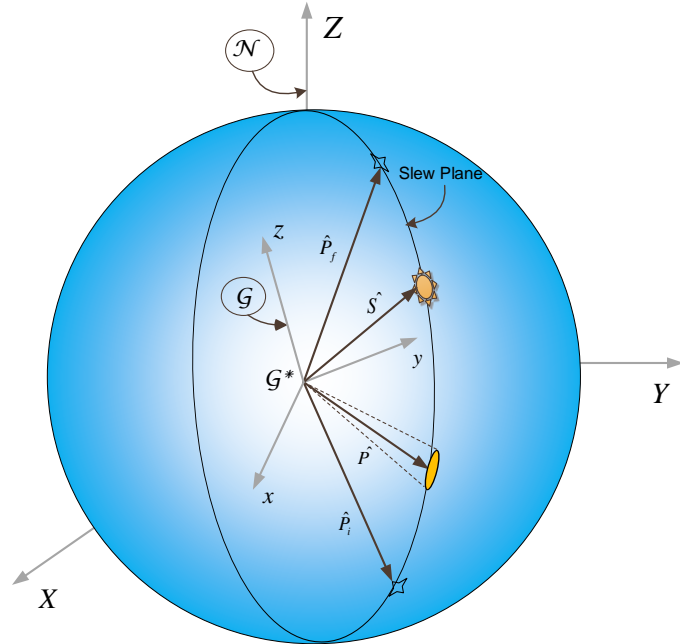


**Fig. 1 Gyrostat-centered unit sphere centered at point  $G^*$ .**

Throughout this paper, the left subscript of a vector denotes the reference frame in which the vector is expressed.

### III. Sun-Avoidance Slew (SAS) Algorithm Description

The first step is to determine if there is a sun vector intrusion. To this end, we check the angular separation,  $\alpha$ , between the sun unit vector,  ${}_N\hat{S}$ , and the  $\hat{P}_i - \hat{P}_f$  plane, or “slew plane,”

$$\alpha = \frac{\pi}{2} - \cos^{-1}(\hat{S} \cdot \hat{e}), \quad (1)$$

where the eigenaxis unit vector is determined by

$$\hat{e} = \frac{\hat{P}_i \times \hat{P}_f}{|\hat{P}_i \times \hat{P}_f|}. \quad (2)$$

If  $|\alpha| \geq \epsilon_p$  then the sun vector intrusion has not occurred. Otherwise, we need to perform the sun-avoidance slew maneuver which is explained in the following.

If  $|\alpha| < \epsilon_p$ , then we need to plan the sun-avoidance slew in the following steps:

- I) The 1<sup>st</sup> slew is around the eigenaxis,  $\hat{e}$ , through angle  $\phi_1$ :

$$\phi_1 = \cos^{-1}(\hat{P}_i \cdot \hat{S}_{||}) - \epsilon_p, \quad (3)$$

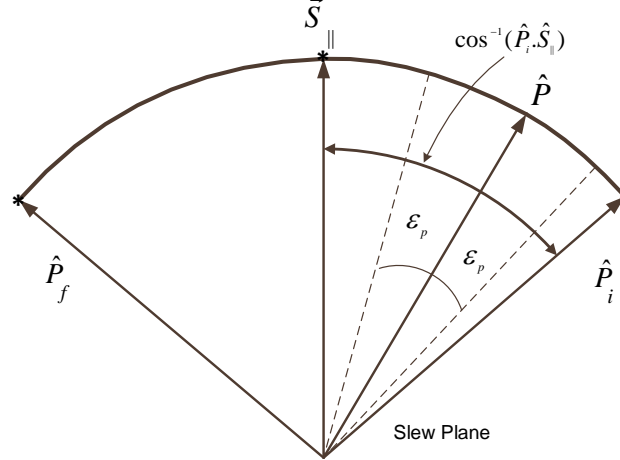


**Fig. 2** View of the sensitive instrument’s LOS vector motion during the 1<sup>st</sup> slew from above the slew plane.

where

$$\vec{S}_{||} = \hat{S} \cos \alpha, \quad (4)$$

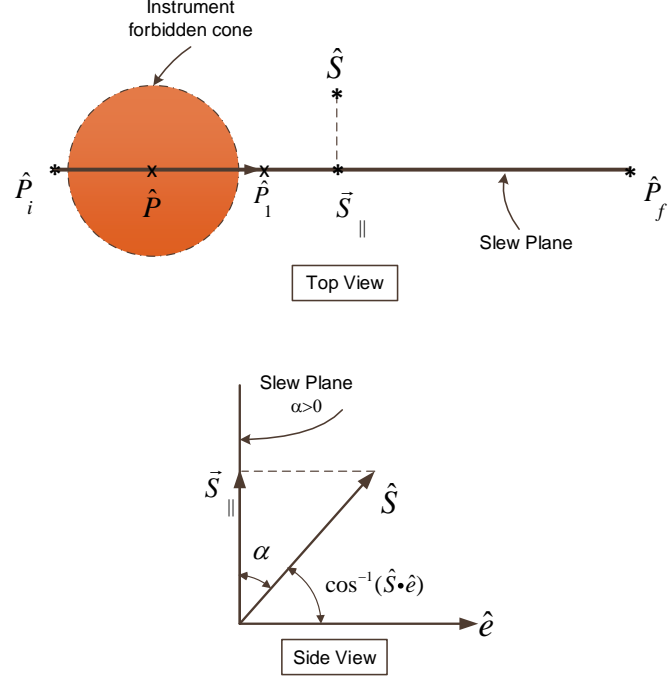


**Fig. 3 Top and side views of the sensitive instrument's LOS vector motion during the 1<sup>st</sup> slew.**

and

$$\hat{S}_{||} = \frac{\vec{S}}{|\vec{S}|}, \quad (5)$$

where vector  $\hat{S}_{||}$  is in the  $\mathcal{N}$ -frame because  $\vec{S}$  is given in the  $\mathcal{N}$ -frame. The vector  $\hat{P}_1$  denotes the position vector of  $\hat{P}$  at the end of 1<sup>st</sup> slew in the  $\mathcal{G}$ -frame.

II) The 2<sup>nd</sup> slew is around the unit sun vector,  $\hat{S}$ , can be found from the spherical triangle  $\hat{P}_1\hat{S}\hat{P}_2$  shown in Fig. 4.

The rotation angle  $\phi_2$ , from  $\hat{P}_1$  to  $\hat{P}_2$  around  $\hat{S}$  is given by[12]

1) when  $\alpha \neq 0$

$$\phi_2 = 2 \tan^{-1} \left[ \frac{\hat{S} \cdot (\mathcal{N}\hat{P}_1 \times \hat{S}_{||})}{(\mathcal{N}\hat{P}_1 \cdot \hat{S}_{||}) - (\hat{S} \cdot \mathcal{N}\hat{P}_1)(\hat{S} \cdot \hat{S}_{||})} \right], \quad (6)$$

or

$$\phi_2 = 2 \tan^{-1} \left( \frac{\sin \alpha \sin \epsilon_p}{\cos \epsilon_p - \cos \theta \cos \alpha} \right). \quad (7)$$

2) when  $\alpha = 0$

$$\phi_2 = \pi. \quad (8)$$

The vector  $\hat{P}_2$  denotes the position vector of  $\hat{P}$  at the end of 2<sup>nd</sup> slew.

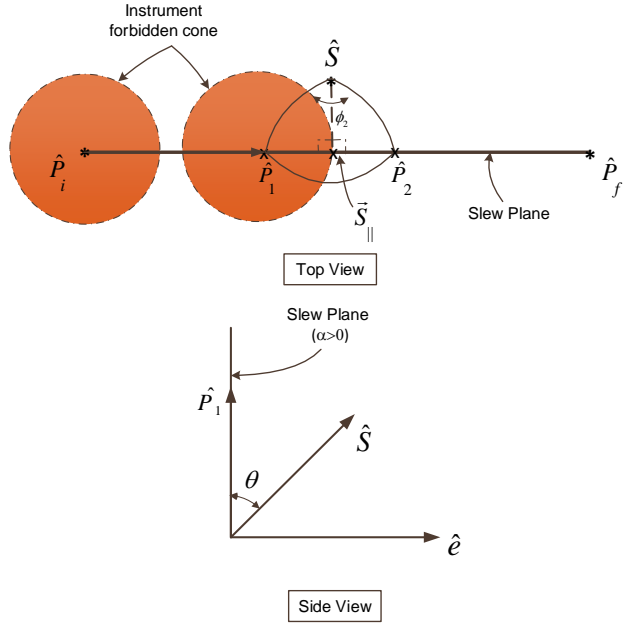


**Fig. 4** The sensitive instrument's LOS vector motion during the 2<sup>nd</sup> slew when  $\alpha \neq 0$ .

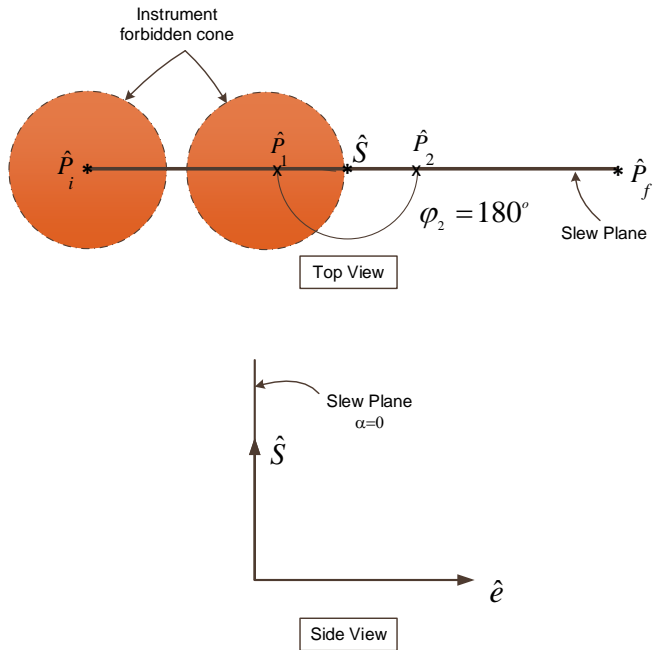


**Fig. 5** The sensitive instrument's LOS vector motion during the 2<sup>nd</sup> slew when  $\alpha = 0$ .

III) The 3<sup>rd</sup> slew is about  $\hat{e}$  through angle  $\phi_3$ :

$$\phi_3 = \cos^{-1}(\hat{P}_f \cdot \hat{S}_{||}) - \epsilon_p. \quad (9)$$

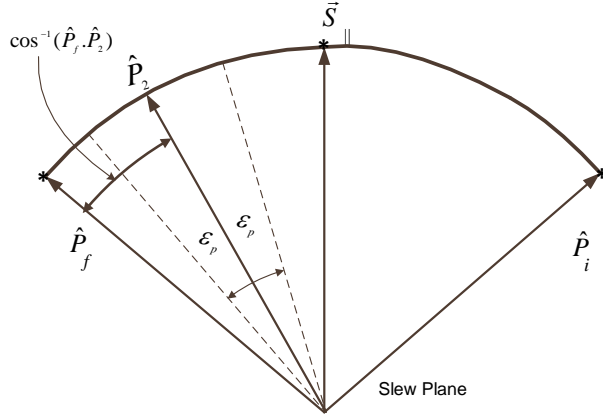


**Fig. 6 The sensitive instrument's LOS vector motion during the 3<sup>rd</sup> slew.**

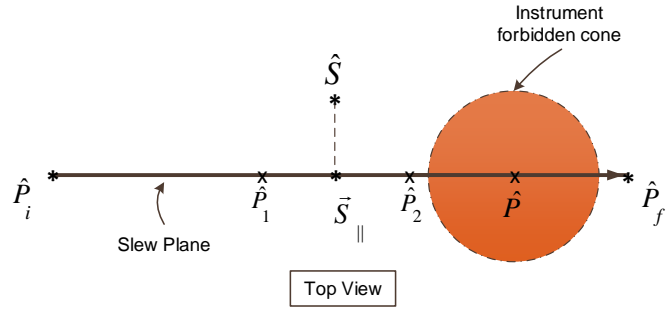


**Fig. 7 Top view of the sensitive instrument's LOS vector motion during the 3<sup>st</sup> slew.**

IV) The final slew about the instrument's LOS axis may be needed to go to the final attitude.

#### Summary of the Sun Avoidance Algorithm:

- 1) Given  $\vec{S}$ ,  $\hat{P}_i$ ,  $\hat{P}_f$ , and  $\epsilon_p$ , compute the angle  $\alpha$ .
- 2) If  $|\alpha| \geq \epsilon_p$  then STOP otherwise go to the next step.
- 3) Slew around the eigenaxis,  $\hat{e}$ , through angle  $\phi_1$ :

$$\phi_1 = \cos^{-1}(\hat{P}_i \cdot \hat{S}_{||}) - \epsilon_p. \quad (10)$$

- 4) Slew around the  $\hat{S}$  via:

$$\phi_2 = \begin{cases} 2 \tan^{-1} \left( \frac{\sin \alpha \sin \epsilon_p}{\cos \epsilon_p - \cos \theta \cos \alpha} \right), & \text{when } \alpha \neq 0 \\ \pi, & \text{when } \alpha = 0 \end{cases} \quad (11)$$

- 5) Slew about  $\hat{e}$  through angle:

$$\phi_3 = \cos^{-1}(\hat{P}_f \cdot \hat{S}_{||}) - \epsilon_p. \quad (12)$$

- 6) If necessary, perform the final rotation,  $\phi_4$ , about the instrument's LOS axis to adjust the attitude.

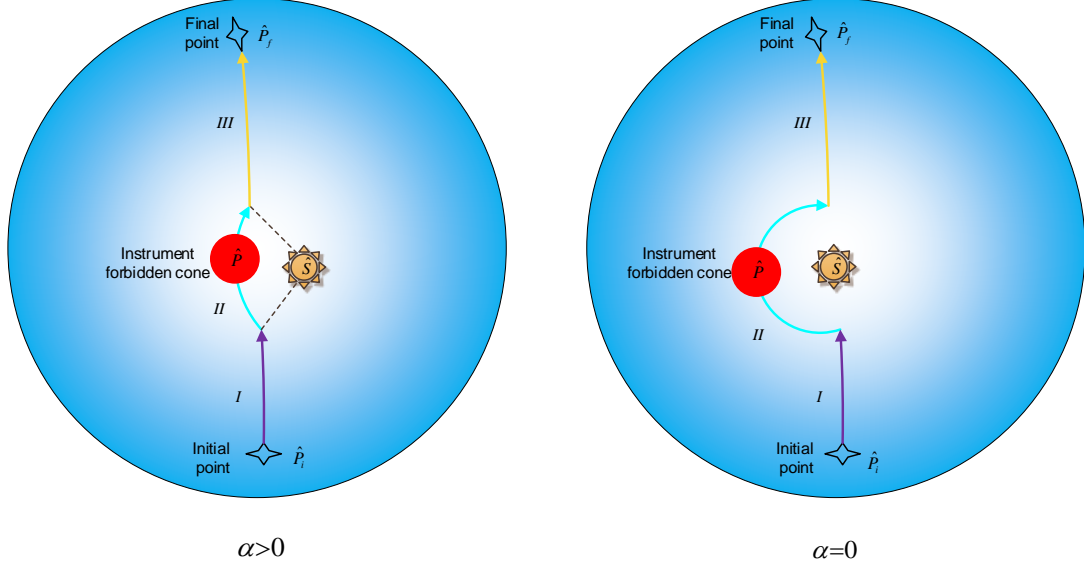


**Fig. 8 The trajectory of the instrument's LOS tip on the gyrostat-centered unit sphere during the SAS maneuver.**

#### IV. Slew Planning

In this section we utilize the proposed sun-avoidance slew algorithm to generate the desired —which we call it through the rest of this paper, “target” ( $\mathcal{T}$ )—attitude in terms of unit quaternions,  ${}^N q^{\mathcal{T}}(t)$ , and the angular rate,  ${}^N \omega^{\mathcal{T}}(t)$ , and angular acceleration,  ${}^N \dot{\omega}^{\mathcal{T}}(t)$ , of the desired (target) frame in the Newtonian ( $N$ ) frame. As it mentioned before, the left subscript of a vector is reserved to denote which reference frame the vector is expressed-in, e.g. both angular rate and acceleration vectors are expressed in the  $\mathcal{G}$ -frame. The block diagram of the slew planning and control loop is shown in Fig. 9. It can be seen from there that the generated commands are utilized by an attitude control system to guide the gyrostat in each segment of the proposed SAS.

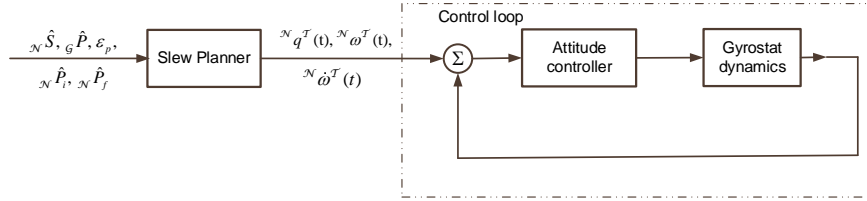


**Fig. 9 Block diagram of control loop.**

In the following, we formulate the problem of slew planning for two cases: 1) velocity and acceleration constraints and 2) acceleration constraint.

### A. Case 1: Single-Axis, Agile Slew Maneuver with Velocity and Acceleration Constraints.

*Problem Statement:* Find the optimal time history of the rotation angle of the  $\mathcal{T}$ -frame around a given inertially-fixed axis,  $\mathcal{N}\hat{e}$ , as shown in Fig. 10.

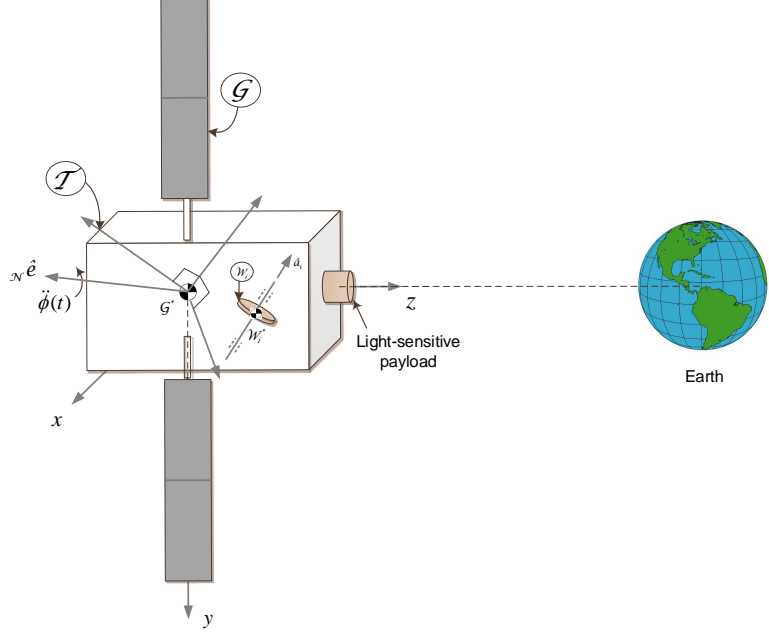


**Fig. 10** A gyrostabilized payload rotating about its eigenaxis,  $\mathcal{N}\hat{e}$ .

The problem of minimum-time slew of  $\mathcal{T}$ -frame around the  $\mathcal{N}\hat{e}$ -axis can be formulated as:

$$\underset{u_{\hat{e}} \in \mathcal{U}}{\text{Minimize}} \mathcal{J}[x(\cdot), u_{\hat{e}}(\cdot), t_f] = \int_{t_0}^{t_f} dt, \quad (13)$$

subject to the following kinematic constraints:

$$\Sigma_{\mathcal{T}} : \begin{cases} \dot{x}_1 = x_2, \\ \dot{x}_2 = u_{\hat{e}}, \end{cases} \quad (14)$$

and,

$$C_1 : \begin{cases} |x_2 - \dot{\phi}| \leq \dot{\phi}_{max}, & (\text{state constraint}) \\ |u_{\hat{e}} - \ddot{\phi}| \leq \ddot{\phi}_{max}, & (\text{control constraint}) \end{cases} \quad (15)$$

with boundary conditions,

$$BCs : \begin{cases} \phi(t_0) = 0, \phi(t_f) = \phi_f, \\ \dot{\phi}(t_0) = \dot{\phi}_0, \dot{\phi}(t_f) = 0, \end{cases} \quad (16)$$

where the input  $u_{\hat{e}}$  is the acceleration around the  $\mathcal{N}\hat{e}$ -axis,  $\mathcal{U}$  is the set of all admissible controls,  $x_1 \triangleq \phi$ , and  $x_2 = \dot{\phi}$ . The objective is to find  ${}^N\omega^T(t)$ ,  ${}^N\dot{\omega}^T(t)$ , and  ${}^Nq^T(t)$ .

Using the optimal control theory and Pontryagin's minimum principle (PMP), we transform the state constraint inequality into a single equality constraint and then to augment it with the state equation[13]. The necessary conditions for the optimal solution can be derived as follows:

1) State Eqs.:

$$\begin{cases} \dot{x}_1 = x_2, \\ \dot{x}_2 = u_{\hat{e}}, \\ \dot{x}_3 = (x_2 + \dot{\phi}_{max})^2 \mathbb{U}(-x_2 - \dot{\phi}_{max}) + (\dot{\phi}_{max} - x_2)^2 \mathbb{U}(x_2 - \dot{\phi}_{max}), \end{cases} \quad (17)$$

where the Heaviside step function,  $\mathbb{U}(.)$ , is defined as

$$\mathbb{U}(X) = \begin{cases} 1, & X > 0, \\ 0, & X \leq 0. \end{cases} \quad (18)$$

It should be noted here that if the constraint is satisfied for all  $t \in [t_0, t_f]$ , which means  $x_3(t) \geq 0$ , and because  $(x_3(t_0) = x_3(t_f) = 0)$  therefore, we have  $x_3(t) = 0$ .

2) Hamiltonian:

$$\mathcal{H} = 1 + \lambda_1 x_2 + \lambda_2 u_{\hat{e}} + \lambda_3 \left[ (x_2 + \dot{\phi}_{max})^2 \mathbb{U}(-x_2 - \dot{\phi}_{max}) + (\dot{\phi}_{max} - x_2)^2 \mathbb{U}(x_2 - \dot{\phi}_{max}) \right]. \quad (19)$$

3) Costate Eqs.:

$$\begin{cases} \dot{\lambda}_1 = -\frac{\partial \mathcal{H}}{\partial x_1} = 0, \\ \dot{\lambda}_2 = -\frac{\partial \mathcal{H}}{\partial x_2} = -\lambda_1 - 2\lambda_3(x_2 + \dot{\phi}_{max})\mathbb{U}(-x_2 - \dot{\phi}_{max}) \\ \quad + 2\lambda_3(\dot{\phi}_{max} - x_2)\mathbb{U}(x_2 - \dot{\phi}_{max}), \\ \dot{\lambda}_3 = -\frac{\partial \mathcal{H}}{\partial x_3} = 0. \end{cases} \quad (20)$$

It is easy to verify the derivation of Eq. (20) because the Heaviside function is either 0 or 1 depends on the sign of its argument.

4) Applying the Pontryagin's minimum principle (PMP),

$$u_{\hat{e}}^* = \arg \min_{u_{\hat{e}} \in \mathcal{U}} \mathcal{H}, \quad (21)$$

where  $\mathcal{U}$  defines the domain of admissible controls. The optimal control can be determined as

$$u_{\hat{e}}^*(t) = \begin{cases} \ddot{\phi}_{max} & \lambda_2 < 0, \\ ? & \lambda_2 = 0, \\ -\ddot{\phi}_{max} & \lambda_2 > 0. \end{cases} \quad (22)$$

This is a *singular arc* optimal control problem.

- 5) Determining the optimal control in the singular arc:

$$\frac{d^2}{dt^2} \left( \frac{\partial \mathcal{H}}{\partial u_{\hat{e}}} \right) = \ddot{\lambda}_2 = 0 \rightarrow \dot{x}_2 = 0 \rightarrow u_{\hat{e}}^* = 0. \quad (23)$$

- 6) Checking the Generalized Legendre-Clebsch condition for optimality:

$$(-1)^2 \frac{\partial}{\partial u_{\hat{e}}} \left[ \frac{d^2}{dt^2} \left( \frac{\partial \mathcal{H}}{\partial u_{\hat{e}}} \right) \right] = 1 \geq 0. \quad (24)$$

- 7) Checking the transversality condition:

$$\mathcal{H}|_{(*, t_f)} = 0 \text{ and } \mathcal{H} \neq \mathcal{H}(t) \rightarrow \mathcal{H} = 0, \forall t \in [t_0, t_f]. \quad (25)$$

The angular acceleration profile is bang-off-bang, as shown in Fig. 11

$$u_{\hat{e}}^*(t) = \ddot{\phi}(t) = \begin{cases} \ddot{\phi}_{max} & \text{when } t_0 \leq t \leq t_1, \\ 0 & \text{when } t_1 \leq t \leq t_2, \\ -\ddot{\phi}_{max} & \text{when } t_2 \leq t \leq t_f. \end{cases} \quad (26)$$

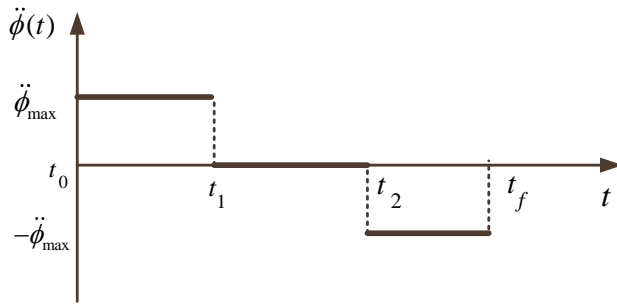


**Fig. 11** The optimal control law for case 1.

The angular velocity profile can be determined as

$$\dot{\phi}(t) = \begin{cases} \dot{\phi}_0 + \ddot{\phi}_{max}(t - t_0) & \text{when } t_0 \leq t \leq t_1, \\ \dot{\phi}_{max} & \text{when } t_1 \leq t \leq t_2, \\ \dot{\phi}_{max} - \ddot{\phi}_{max}(t - t_2) & \text{when } t_2 \leq t \leq t_f. \end{cases} \quad (27)$$

and the angular position can be find by direct integration of Eq. (27),

$$\phi(t) = \begin{cases} \dot{\phi}_0(t - t_0) + \frac{1}{2}\ddot{\phi}_{max}(t - t_0)^2 & \text{when } t_0 \leq t \leq t_1, \\ \phi(t_1) + \dot{\phi}_{max}(t - t_1) & \text{when } t_1 \leq t \leq t_2, \\ \phi(t_2) + \dot{\phi}_{max}(t - t_2) - \frac{1}{2}\ddot{\phi}_{max}(t - t_2)^2 & \text{when } t_2 \leq t \leq t_f. \end{cases} \quad (28)$$

Using the conditions,  $\dot{\phi}(t_1) = \dot{\phi}_{max}$ ,  $\dot{\phi}(t_f) = 0$ ,  $\phi(t_f) = \phi_f$ , we can determine switching times  $t_1$ ,  $t_2$ , and final time  $t_f$ . Depending on the magnitude of  $\phi$  and the maximum velocity and acceleration constraints, the target frame may or may not reach its maximum allowed velocity during a slew, which in turn determines the calculation of switching times. There is a threshold angle, which is called  $\phi_t$  and is calculated from the constraints:

$$\phi_t = \frac{\dot{\phi}_{max}^2}{\ddot{\phi}_{max}}. \quad (29)$$

If  $\phi > \phi_t$ , then there will be period of coasting at constant velocity (at the maximum velocity constraint) in between the periods of acceleration and deceleration during the slew. In such a case, we can determine switching times  $t_1$ ,  $t_2$ , and final time  $t_f$  as

$$t_1 = t_0 + \frac{\dot{\phi}_{max} - \dot{\phi}_0}{\ddot{\phi}_{max}}, \quad (30)$$

$$t_2 = t_1 + \frac{1}{\dot{\phi}_{max}} \left[ \phi_f - \dot{\phi}_0(t_1 - t_0) - \frac{1}{2}\ddot{\phi}_{max}(t_1 - t_0)^2 - \frac{\dot{\phi}_{max}^2}{2\ddot{\phi}_{max}} \right], \quad (31)$$

and

$$t_f = t_1 + \frac{1}{\dot{\phi}_{max}} \left[ \phi_f - \dot{\phi}_0(t_1 - t_0) - \frac{1}{2}\ddot{\phi}_{max}(t_1 - t_0)^2 + \frac{\dot{\phi}_{max}^2}{2\ddot{\phi}_{max}} \right]. \quad (32)$$

Otherwise, if  $\phi \leq \phi_t$ , then there will be no period of coasting at angular velocity, and the acceleration profile of the target frame will be changing from the initial to the final point of the slew. The switching times are then determined by:

$$t_f = \sqrt{\frac{4\phi}{\ddot{\phi}_{max}}}, \quad (33)$$

$$t_2 = \frac{t_f}{2}, \quad (34)$$

$$t_1 = t_2. \quad (35)$$

Assume  ${}_N\hat{e} = (e_X, e_Y, e_Z)$  and that the  $\mathcal{T}$ - and  $\mathcal{N}$ -frames are coincident at  $t_0$ . Then the target steering profiles including the unit quaternions of  $\mathcal{T}$  in  $\mathcal{N}$ , and the angular rate and angular acceleration of the  $\mathcal{T}$ -frame in  $\mathcal{N}$ -frame can be determined as

$${}^N q^{\mathcal{T}}(t) = \left[ e_X \sin \frac{\phi(t)}{2}, e_Y \sin \frac{\phi(t)}{2}, e_Z \sin \frac{\phi(t)}{2}, \cos \frac{\phi(t)}{2} \right]^T, \quad (36)$$

$${}^N \omega^{\mathcal{T}} = \dot{\phi}(t) [{}^G R^N] {}_N \hat{e}, \quad (37)$$

$${}^N \ddot{\omega}^{\mathcal{T}} = \ddot{\phi}(t) [{}^G R^N] {}_N \hat{e}. \quad (38)$$

Note that the computed  ${}^N \omega^{\mathcal{T}}$  and  ${}^N \ddot{\omega}^{\mathcal{T}}$  given by Eqs. (37)–(38) are expressed in the  $\mathcal{G}$ -frame. The required equivalent wheel torque,  ${}_G u_r \in \mathbb{R}^{3 \times 1}$ , along the gyrostat body axes can be determined from the Euler rotational equations of motion as

$${}_G u_r = [{}^G J^{\mathcal{G}/\mathcal{G}^*}] {}_G \dot{\omega}^{\mathcal{T}} + [{}^N \omega^{\mathcal{T}}]^{\times} [{}^G J^{\mathcal{G}/\mathcal{G}^*}] {}_G \omega^{\mathcal{T}}, \quad (39)$$

where  $[{}^G J^{\mathcal{G}/\mathcal{G}^*}]$  is the moment of inertia of the gyrostat including the moment of inertia of the body and reaction wheels transverse to their spin axes, but not along their spin axes. Then, Euler's rotational equations of motion and the kinematics differential equation for the gyrostat can be rewritten in the form of [14]

$${}^N \dot{\omega}^{\mathcal{G}} = [{}^G J^{\mathcal{G}/\mathcal{G}^*}]^{-1} \left( {}_G u_r - [{}^N \omega^{\mathcal{G}}]^{\times} [{}^G J^{\mathcal{G}/\mathcal{G}^*}] {}_G \omega^{\mathcal{G}} \right), \quad (40)$$

$${}^N \dot{h}^{\mathcal{W}/\mathcal{W}^*} = -{}_G u_r - [{}^N \omega^{\mathcal{G}}]^{\times} [{}^N h^{\mathcal{W}/\mathcal{W}^*}], \quad (41)$$

$${}^N \dot{q}^{\mathcal{G}} = \frac{1}{2} [\Omega({}^N \omega^{\mathcal{G}})] {}^N q^{\mathcal{G}}, \quad (42)$$

where  ${}^N \dot{\omega}^{\mathcal{G}}$  is the angular velocity of the gyrostat with respect to the  $\mathcal{N}$ -frame and  ${}^N \dot{h}^{\mathcal{W}/\mathcal{W}^*}$  is the total angular momentum of reaction wheel assembly expressed in the  $\mathcal{G}$ -frame.

$$[\Omega({}^N \omega^{\mathcal{G}})] = \begin{bmatrix} 0 & \omega_z & -\omega_y & \omega_x \\ -\omega_z & 0 & -\omega_x & \omega_y \\ \omega_y & -\omega_x & 0 & \omega_z \\ -\omega_x & \omega_y & -\omega_z & 0 \end{bmatrix}, \quad (43)$$

$${}^N \omega^{\mathcal{G}} = (\omega_x, \omega_y, \omega_z), \quad (44)$$

f and

$${}_{\mathcal{G}}^N h^{\mathcal{W}/\mathcal{W}^*} = (h_x, h_y, h_z). \quad (45)$$

The unit quaternion,  ${}^N q^{\mathcal{G}}$ , has three-vector parts  $(q_1, q_2, q_3)$  and a scalar part  $q_4$  and it is defined as

$${}^N q^{\mathcal{G}} = [q_1, q_2, q_3, q_4]^T. \quad (46)$$

The total angular momentum of the reaction wheels,  ${}_{\mathcal{G}}^N h^{\mathcal{W}/\mathcal{W}^*}$ , can be calculated from

$${}_{\mathcal{G}}^N h^{\mathcal{W}/\mathcal{W}^*} = \mathcal{A}_m [J_s] (\omega_s + \mathcal{A}_m^T {}_{\mathcal{G}}^N \omega^{\mathcal{G}}), \quad (47)$$

where the mounting matrix of  $m$  reaction wheels,  $\mathcal{A}_m \in \mathbb{R}^{3 \times m}$ , is formed by the unit vectors,  $\hat{a}_i$ ; ( $i = 1, \dots, m$ ), along  $i^{th}$  wheel's spin axis in the  $\mathcal{G}$ -frame.

$$\mathcal{A}_m = [\hat{a}_1 \ \hat{a}_2 \ \dots \ \hat{a}_m]. \quad (48)$$

Furthermore, in Eq. (47), the  $\omega_s$  and  $[J_s]$  are defined as

$$\omega_s = [\omega_{s1}, \omega_{s2}, \dots, \omega_{sm}]^T, \quad (49)$$

and

$$[J_s] = \text{diag}(J_{s1}, J_{s2}, \dots, J_{sm}), \quad (50)$$

where  $\text{diag}(\cdot)$  denotes diagonal matrix,  $J_{si}$  and  $\omega_{si}$  are the moment of inertia along the spin axis, and spin rate of the  $i^{th}$  wheel, respectively. In practice, the angular momentum storage capacity and torque of the individual wheels in the wheel's frame of reference are known. The angular momentums and torques for the whole wheel assembly can be transformed from the wheel to the gyrostat frame by

$${}_{\mathcal{G}}^N h^{\mathcal{W}/\mathcal{W}^*} = \mathcal{A}_m {}_{\mathcal{W}}^N h^{\mathcal{W}/\mathcal{W}^*}, \quad {}_{\mathcal{G}} u_r = \mathcal{A}_m {}_{\mathcal{W}} u_r, \quad (51)$$

or from the gyrostat to the wheel frames by using the pseudoinverse distribution law as

$${}_{\mathcal{W}}^N h^{\mathcal{W}/\mathcal{W}^*} = \mathcal{A}_m^\dagger {}_{\mathcal{G}}^N h^{\mathcal{W}/\mathcal{W}^*}, \quad {}_{\mathcal{W}} u_r = \mathcal{A}_m^\dagger {}_{\mathcal{G}} u_r. \quad (52)$$

The symbol  $\dagger$  denotes the pseudoinverse or Moore-Penrose generalized inverse of a real matrix which is defined as

$$\mathcal{A}_m^\dagger = \mathcal{A}_m^T (\mathcal{A}_m \mathcal{A}_m^T)^{-1}. \quad (53)$$

It can be shown that the angular momentum of reaction wheels with respect to the wheel frame,  ${}^W_h {}^{W/W^*}$ , can be found from Eq. (47) as follows

$${}^W_h {}^{W/W^*} = (\mathcal{A}_m^T \mathcal{A}_m)^{-1} \mathcal{A}_m^T {}^N_h {}^{W/W^*} - [J_s] \mathcal{A}_m^T {}^N \omega^G, \quad (54)$$

where

$${}^W_h {}^{W/W^*} = [J_s] \omega_s. \quad (55)$$

It is worth noting that the upper bounds in Eq. (15) should be carefully chosen in such a way that it does not violate the wheels angular momentum storage capacity and wheel torque constraints. These constraints can be checked by using Eqs. (39) and (54). In the next section, we consider a simpler case when we only have acceleration constraint on the gyrostat.

### B. Case 2: Single-Axis, Agile Slew Maneuver with Acceleration Constraint

*Problem Statement:* Consider the optimal control problem described by Eqs. (13), (14), and (16), subject to the acceleration constraint

$$C_2 : |u = \ddot{\phi}| \leq \ddot{\phi}_{max}. \quad (56)$$

Find  ${}^N\omega^T(t)$ ,  ${}^N\dot{\omega}^T(t)$ , and  ${}^Nq^T(t)$  for the SAS maneuver.

It is well known result that in this case the angular acceleration about  $\hat{e}$  axis is a bang-bang control as shown in Fig. 12.

$$\ddot{\phi}(t) = \ddot{\phi}_{max} \mathbb{U}(t_0) - 2\ddot{\phi}_{max} \mathbb{U}(t - t_1), \quad (57)$$

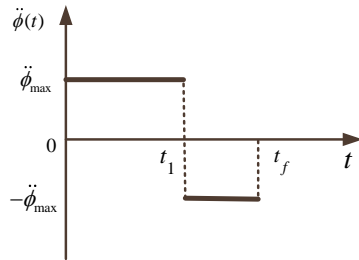


**Fig. 12** The optimal control in case 2.

where the switching and the final times are given by

$$t_1 = t_0 - \frac{\dot{\phi}_0}{\ddot{\phi}_{max}} + \frac{\sqrt{\ddot{\phi}_{max}^2(2\ddot{\phi}_{max}\phi_f + \dot{\phi}_0^2)}}{\sqrt{2}\ddot{\phi}_{max}}, \quad (58)$$

and

$$t_f = t_0 - \frac{\dot{\phi}_0}{\ddot{\phi}_{max}} + \frac{\sqrt{2}\sqrt{\ddot{\phi}_{max}^2(2\ddot{\phi}_{max}\phi_f + \dot{\phi}_0^2)}}{\ddot{\phi}_{max}^2}. \quad (59)$$

The angular velocity and angular rate about  $\hat{e}$  axis are

$$\dot{\phi}(t) = \dot{\phi}_0 + \ddot{\phi}_{max}(t - t_0)\mathbb{U}(t_0) - 2\ddot{\phi}_{max}(t - t_1)\mathbb{U}(t - t_1), \quad (60)$$

$$\phi(t) = \dot{\phi}_0(t - t_0) + \ddot{\phi}_{max}\frac{(t - t_0)^2}{2}\mathbb{U}(t_0) - 2\ddot{\phi}_{max}\frac{(t - t_1)^2}{2}\mathbb{U}(t - t_1). \quad (61)$$

### 1. The First Slew Maneuver:

This is a single-axis nonrest-to-rest maneuver around  $\hat{e}$  with the boundary conditions

$$\dot{\phi}(t_0) = \dot{\phi}_0, \phi(t_0) = 0, \dot{\phi}(t_{f1}) = 0, \phi(t_{f1}) = \phi_1. \quad (62)$$

The switching time,  $t_{11}$ , and the minimum-time,  $t_{f1}$ , are

$$t_{11} = t_0 - \frac{\dot{\phi}_0}{\ddot{\phi}_{max}} + \frac{\sqrt{\ddot{\phi}_{max}^2(2\ddot{\phi}_{max}\phi_1 + \dot{\phi}_0^2)}}{\sqrt{2}\ddot{\phi}_{max}}, \quad (63)$$

$$t_{f1} = t_0 - \frac{\dot{\phi}_0}{\ddot{\phi}_{max}} + \frac{\sqrt{2\ddot{\phi}_{max}^2(2\ddot{\phi}_{max}\phi_1 + \dot{\phi}_0^2)}}{\ddot{\phi}_{max}}. \quad (64)$$

### 2. The Second Slew Maneuver:

This is a rest-to-rest maneuver around the sun vector with boundary conditions given by

$$\dot{\phi}(t_0) = 0, \phi(t_0) = 0, \dot{\phi}(t_{f2}) = 0, \phi(t_{f2}) = \phi_2. \quad (65)$$

The switching time,  $t_{12}$ , and the minimum-time,  $t_{f2}$ , are

$$t_{12} = t_0 - \frac{\sqrt{\phi_2}}{\ddot{\phi}_{max}}, \quad (66)$$

$$t_{f2} = t_0 - \frac{2\sqrt{\phi_2}}{\ddot{\phi}_{max}}. \quad (67)$$

### 3. The Third Slew Maneuver:

This is a single-axis rest-to-rest maneuver around  $\hat{e}$  with the boundary conditions

$$\dot{\phi}(t_0) = 0, \phi(t_0) = 0, \dot{\phi}(t_{f3}) = 0, \phi(t_{f3}) = \phi_3. \quad (68)$$

The switching time,  $t_{13}$ , and the minimum-time,  $t_{f3}$ , are

$$t_{13} = t_0 + \sqrt{\phi_3 / \ddot{\phi}_{max}}, \quad (69)$$

$$t_{f3} = t_{13}. \quad (70)$$

Knowing the switching times for each slew, the  $\ddot{\phi}(t)$ ,  $\dot{\phi}(t)$ , and  $\phi(t)$  can be found by substituting the boundary conditions for each slew into Eqs. (57), (60), and (61), respectively. Then the steering profiles, i.e.  ${}^N\omega^T(t)$ ,  ${}^N\dot{\omega}^T(t)$ , and  ${}^Nq^T(t)$  can be determined from Eqs. (36)–(38).

## V. Numerical simulation

We used MATLAB® to examine and validate the proposed algorithm in this paper. The initial, final, and sun position vectors were selected randomly such that the initial and final positions end up outside of the exclusion zone. The progression of the gyrostat along its orbit was not incorporated in these simulations, therefore, the sun vector does not change during the slew maneuvers. However, when the orbit is taken into account during real missions, the location of the sun vector during the  $\phi_2$  portion of the maneuvers should be considered. Or rather, the timing of the instrument's LOS overlapping with the sun vector projection onto the slew plane should be used in the calculation of the slew angles. The pseudocode for the proposed SAS planning is shown Algorithm 1.

In the following, we present the results of two cases: I) when the sun angle does not lie in the slew plane,  $|\alpha| > 0$ , and II) when the sun vector lies in the slew plane,  $\alpha = 0$ . The parameters used in both cases are listed in Table 1. In case I, when  $|\alpha| > 0$ , the gyrostat slews from the initial to the target position during the maneuvers, and  $P_1$  and  $P_2$  are connected via a rotation around the sun vector as shown in Fig. 13.

We chose a symmetric pyramid configuration with four identical reaction wheel,  $m = 4$ , for this simulation. The reaction wheels are configured such that the mounting matrix, which relates the spin axis of each individual wheel to the

---

**Algorithm 1** A Pseudocode for the Sun-Avoidance Slew Planning

---

```

1: Find eigenaxis,  $\mathcal{N}\hat{e}$ , of the slew plane.
2: Compute cross product of  $\hat{P}_i$  and  $\hat{P}_f$  unit vectors.
3: Compute angle between sun vector and slew plane angle  $\alpha$ .
4: if  $|\alpha| < \epsilon_p$  then
5:   Execute sun-avoidance slew:
6:   Find  $\vec{S}_{||}$ .
7:   Compute  $\phi_1, \phi_2, \phi_3$ .
8:   Compute  $\phi_t$ .
9:   Compute the achievable momentum vector in the gyrostat frame.
10:  Use the mounting matrix and individual wheel momentum in Eqs (51), (54), and (55).
11:  Select  $\dot{\phi}_{max}, \ddot{\phi}_{max}$  such that available momentum from reaction wheels is not violated
12:  Compute switching times  $t_1, t_2, t_f$  for  $\phi_1, \phi_2$ , and  $\phi_3$ .
13:  if  $\phi > \phi_t$  then
14:    Use Eqs. (30)–(32)
15:  else
16:    Use Eqs. (33)–(35).
17:  end if
18:  for  $t_0 < t < t_1$  do
19:    Use Eqs. (36)–(38) and  $\mathcal{G}R^N$ , to determine  $\mathcal{N}q^T, \mathcal{N}\omega^T$ , and  $\mathcal{N}\dot{\omega}^T$ .
20:    Compute the required body-fixed torque from Eq. (39).
21:    if  $\|\mathcal{G}u_r\|_\infty \geq \|\bar{u}_a\|_\infty$  then
22:      Go to step 9
23:    else
24:      Propagate  $\mathcal{N}\omega^G, \mathcal{N}h^{w/w^*}$ , and  $\mathcal{N}q^G$  by solving Eqs. (40)–(42).
25:      Use Eq. (54) to check that  $\mathcal{N}h^{w/w^*}$  for each wheel does not exceed momentum storage capacity
         calculated in step 9.
26:    end if
27:  end for
28:  Repeat above lines for  $t_1 < t < t_2$  and  $t_2 < t < t_f$ .
29: else
30:   Slew directly from  $P_i$  to  $P_f$ .
31: end if
```

Note:  $\|\cdot\|_\infty$  denotes  $\infty$ -norm of a vector.

---

gyrostat frame axes, is given by

$$\mathcal{A}_4 = \begin{bmatrix} \sqrt{2}/2 \sin(\gamma) & \sqrt{2}/2 \sin(\gamma) & -\sqrt{2}/2 \sin(\gamma) & -\sqrt{2}/2 \sin(\gamma) \\ -\sqrt{2}/2 \sin(\gamma) & \sqrt{2}/2 \sin(\gamma) & -\sqrt{2}/2 \sin(\gamma) & \sqrt{2}/2 \sin(\gamma) \\ \cos(\gamma) & \cos(\gamma) & \cos(\gamma) & \cos(\gamma) \end{bmatrix}, \quad (71)$$

where the angle  $\gamma$ , which represents the angle between the spin axis of the wheel and the z axis of the gyrostat frame, is set to  $65^\circ$  for these simulations.

The total angular momentum storage capacity of each individual wheel,  $\mathcal{W}h^{w/w^*}$ , was chosen to be  $12 \text{ Nms}$ . The

**Table 1 Initial, Final, and Sun Positions in Inertial Frame and Constraints Used in the Simulation**

Case	Symbol	Unit Vector	$\dot{\phi}_{max}$	$\ddot{\phi}_{max}$
I)	$\hat{P}_i$	[−0.50, 0.57, 0.65]		
	$\hat{P}_f$	[0.76, −0.48, −0.44]	0.0873 (rad/s)	0.0524 (rad/s <sup>2</sup> )
	$\hat{S}$	[0.30, −0.50, −0.81]		
II)	$P_i$	[0.65, −0.35, −0.67]		
	$P_f$	[-0.93, -0.25, 0.28]	0.01 (rad/s)	0.02 (rad/s <sup>2</sup> )
	$S$	[-0.20, -0.78, -0.59]		

gyrostat and wheel moment of inertias are given by

$$\mathcal{G}J^{\mathcal{G}/\mathcal{G}^*} = \begin{bmatrix} 100 & 0 & 0 \\ 0 & 100 & 0 \\ 0 & 0 & 100 \end{bmatrix} (\text{kg.m}^2) \quad J_s = \begin{bmatrix} 0.0019 & 0 & 0 & 0 \\ 0 & 0.0019 & 0 & 0 \\ 0 & 0 & 0.0019 & 0 \\ 0 & 0 & 0 & 0.0019 \end{bmatrix} (\text{kg.m}^2) \quad (72)$$

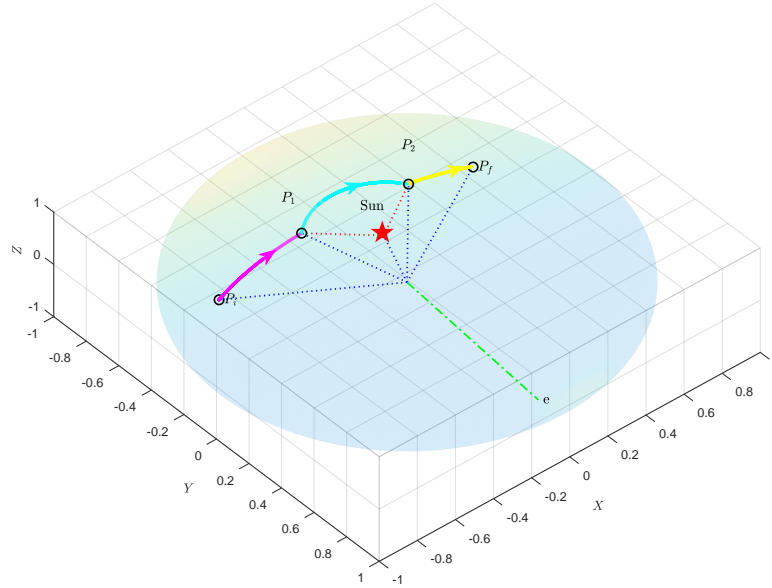


**Fig. 13 Normalized trajectory of the tip of instrument's boresight during the entire slew when  $|\alpha| > 0$ .**

The computed slew angles for Case I are  $(32.08, 102.56, 17.76)^\circ$ . The time histories of angular velocity and angular acceleration are shown in Fig. 14. In real missions, the gyrostat's reaction wheels' ability to impart angular momentum is translated to a constraint in angular velocity, and the thrusters ability to impose torque is translated to a constraint

in angular acceleration. Therefore, no torque constraint is plotted in these results. There are periods of zero angular

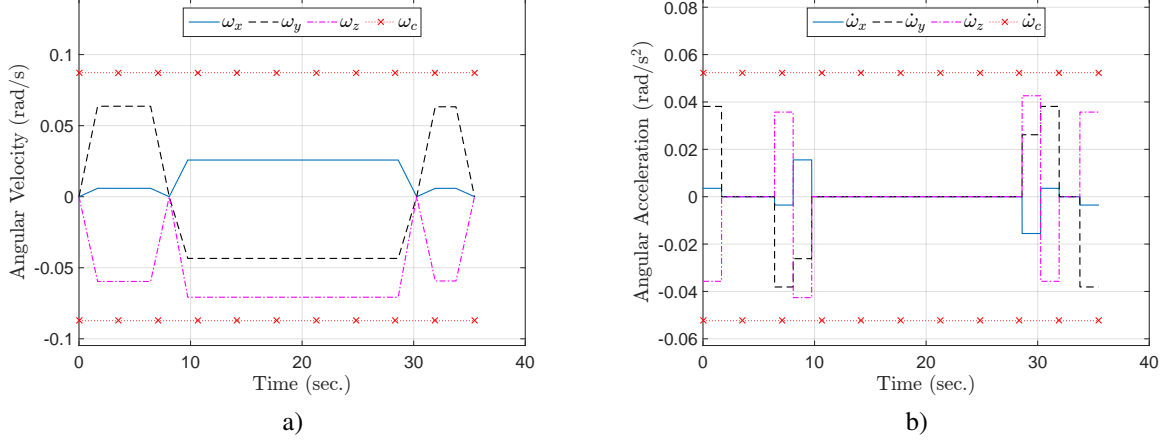


**Fig. 14 Time histories of gyrostat a) angular velocity and b) angular acceleration when  $|\alpha| > 0$ .**

acceleration and constant angular velocity for slew angles, which is reflected in Fig. 14, and which never exceed the constraints defined at the beginning of the simulation. The angular momentum imparted by the wheel assembly on the spacecraft also never exceeds the momentum storage capacity. The time histories of quaternion and body-torque are shown in Fig. 15.

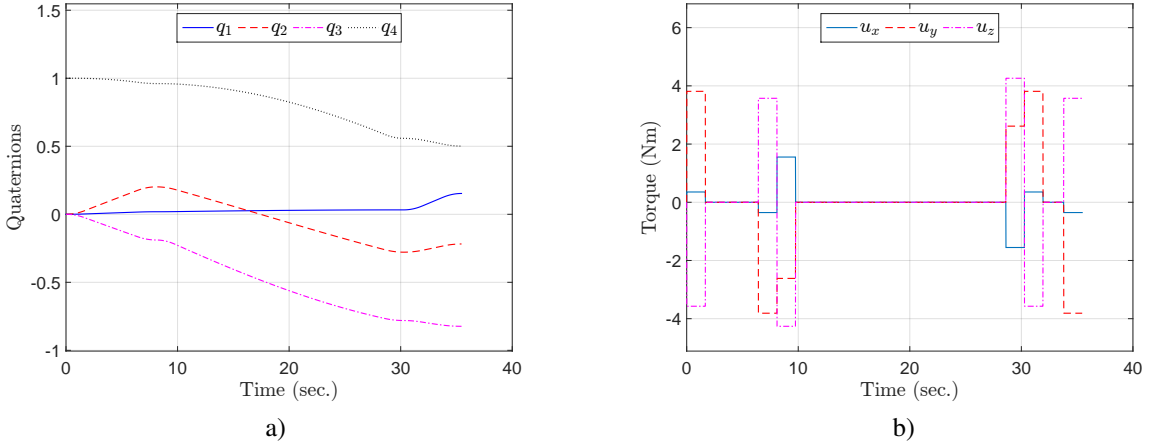


**Fig. 15 Time histories of a) quaternions of  $G$  in  $N$  frame and b) body-fixed torques when  $|\alpha| > 0$ .**

In case II, when  $\alpha = 0$ , we choose much tighter constraints: 0.01 rad/s for angular velocity, and 0.02 rad/s<sup>2</sup> for angular acceleration. The computed slew angles in this case are  $(41.82, 180, 62.45)^\circ$ . The trajectory of the instrument's LOS is shown in Fig. 17. With smaller constraints, the body torque is applied for a very short amount of time before the spacecraft reaches the angular velocity limit. Therefore the period of coasting is increased and the simulation takes longer to complete the slew maneuvers. The maneuver time duration can be adjusted by changing the velocity and acceleration constraints as well as changing the initial, final, and sun vector positions. Figures 18 and 20 show that the

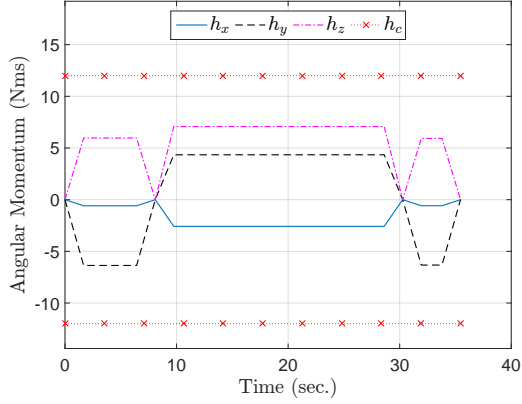


**Fig. 16** Time history of total wheel assembly momentum when  $|\alpha| > 0$ .

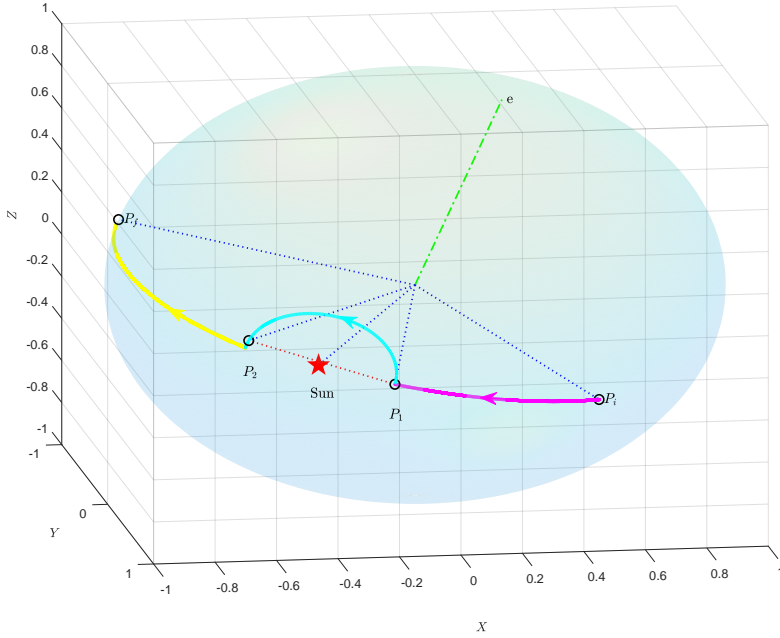


**Fig. 17** Normalized trajectory of the tip of instrument's boresight during the entire slew when  $\alpha = 0$ .

torque and acceleration applied are very short compared to the duration of the entire maneuver for case I ( $|\alpha| > 0$ ), in contrast to Figs. 14 and 15 for case II ( $\alpha = 0$ ). The gyrostat spends the majority of the time coasting at constant angular velocity, as seen in Fig. 18. Though the initial and final points are further apart in the gyrostat unit sphere to begin with, the simulation takes an order of magnitude longer to complete at almost 500 seconds for  $\alpha = 0$ , as opposed to about 5.5 seconds for  $|\alpha| > 0$ . The case shown here is an example that with much tighter constraints and longer maneuver duration. A possible critical mission impact is that the spacecraft, if in a low orbit with high orbital velocity, could see the sun vector change with respect to the gyrostat frame during the slew. Thus, the spacecraft angular velocity and acceleration constraints should be chosen in such a way that the wheel momentum constraints are not violated and the

slew can be completed while the sun vector is as close to its original position as possible.

The results for both cases demonstrate that the angular velocity, acceleration, and wheel momentum never exceed the velocity, acceleration, and wheel momentum constraints for any axis.

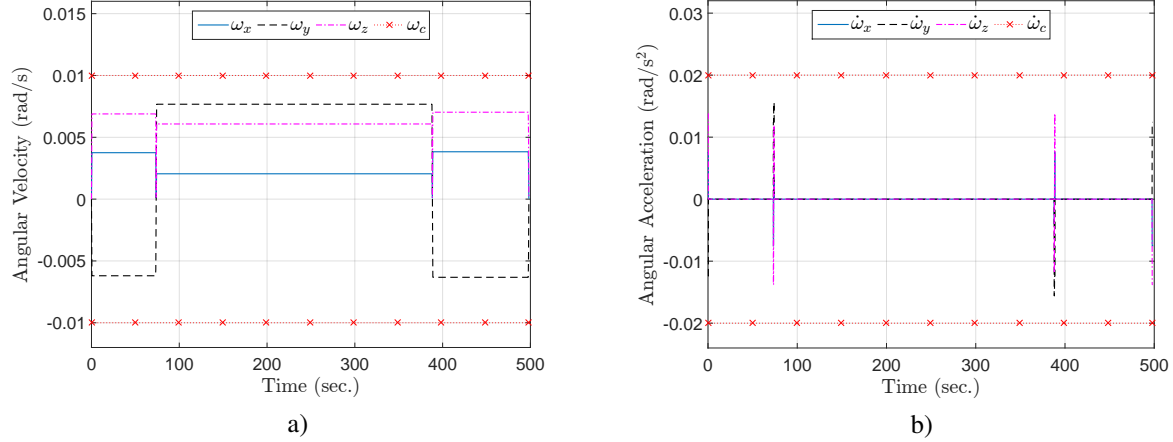


**Fig. 18** Time histories of gyrostat a) angular velocity and b) angular acceleration when  $\alpha = 0$ .

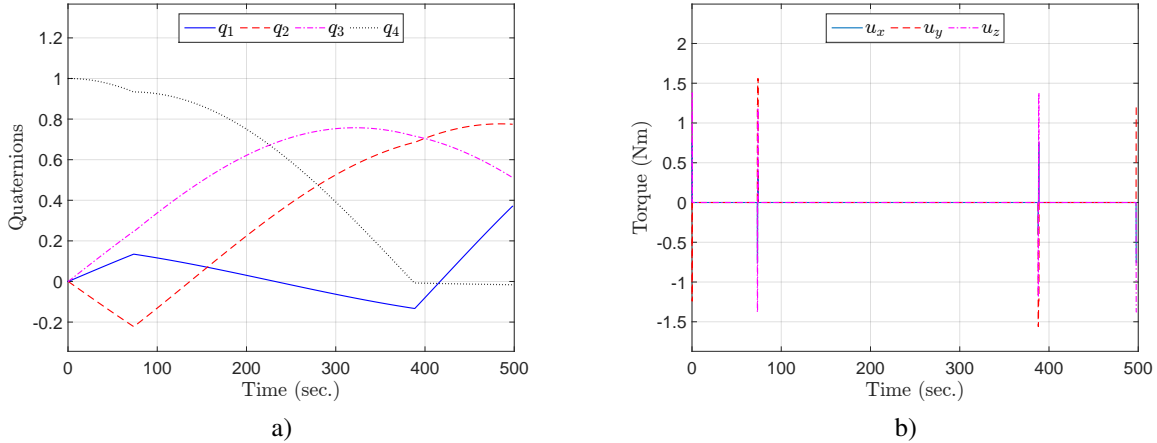


**Fig. 19** Time histories of a) quaternions of  $G$  in  $N$  frame and b) body torques when  $\alpha = 0$ .

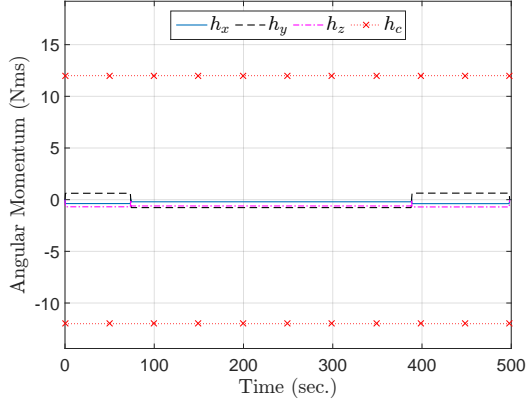


**Fig. 20** Time history of total wheel assembly momentum when  $\alpha = 0$ .

## VI. Conclusion

A new geometric approach for large-angle slew planning with pointing and actuator constraints is presented. The gyrostat has a single light-sensitive payload with control-torque and reaction wheels' angular momentum storage capacity constraints. Furthermore, we assume that the initial and final attitudes, instrument's line-of-sight vector, and sun vector are known. Then the quaternions, angular velocities, and angular accelerations of the desired or target frame are derived based on the PMP. The proposed algorithm is time-optimal, intuitive, closed-form, and easy to implement. The main drawback of the proposed algorithm is its limitation for a single sensitive-payload. The feasibility of the proposed algorithm is demonstrated for two arbitrary cases and it has been investigated via extensive numerical simulations.

## VII. Acknowledgment

This research is supported by Maxar Space Infrastructure (Formerly Space Systems/Loral). The authors would like to acknowledge Luke DeGalan for his useful comments. We thank the anonymous reviewers for their careful reading of the manuscript and their many insightful comments and suggestions.

## References

- [1] R. McInnes, C., “Large angle slew maneuvers with autonomous sun vector avoidance,” *Journal of Guidance Control Dynamics*, Vol. 17, 1994, pp. 875–877. <https://doi.org/10.2514/3.21283>.
- [2] Spindler, K., “New Methods in On-Board Attitude Control,” *Spaceflight Dynamics 1998, Volume 100 Part 1, Advances in Astronautical Sciences*, Vol. 100, edited by T. H. Stengle, 1998, p. 111. URL <https://ui.adsabs.harvard.edu/abs/1998spdy.conf.111S>.
- [3] Hablani, H. B., “Attitude commands avoiding bright objects and maintaining communication with ground station,” *Advances in the Astronautical Sciences*, 1998. <https://doi.org/10.2514/2.4469>.

- [4] Biggs, J. D., and Colley, L., “Geometric Attitude Motion Planning for Spacecraft with Pointing and Actuator Constraints,” *Journal of Guidance, Control, and Dynamics*, 2016. <https://doi.org/10.2514/1.G001514>.
- [5] Feron, E., Dahleh, M., Frazzoli, E., and Kornfeld, R., *A randomized attitude slew planning algorithm for autonomous spacecraft*, chapter and pages. <https://doi.org/10.2514/6.2001-4155>.
- [6] Spiller, D., Ansalone, L., and Curti, F., “Particle Swarm Optimization for Time-Optimal Spacecraft Reorientation with Keep-Out Cones,” *Journal of Guidance, Control, and Dynamics*, 2016. <https://doi.org/10.2514/1.G001228>.
- [7] Kim, Y., and Mesbahi, M., “Quadratically constrained attitude control via semidefinite programming,” *IEEE Transactions on Automatic Control*, 2004. <https://doi.org/10.1109/TAC.2004.825959>.
- [8] Kim, Y., Mesbahi, M., Singh, G., and Hadaegh, F. Y., “On the convex parameterization of constrained spacecraft reorientation,” *IEEE Transactions on Aerospace and Electronic Systems*, 2010. <https://doi.org/10.1109/TAES.2010.5545176>.
- [9] Sun, C., and Dai, R., *Spacecraft Attitude Control under Constrained Zones via Quadratically Constrained Quadratic Programming*, chapter and pages. <https://doi.org/10.2514/6.2015-2010>.
- [10] Lee, U., and Mesbahi, M., “Quaternion based optimal spacecraft reorientation under complex attitude constrained zones,” *Advances in the Astronautical Sciences*, Vol. 150, 2014, pp. 1995–2010.
- [11] Diaz Ramos, M., and Schaub, H., “Kinematic Steering Law for Conically Constrained Torque-Limited Spacecraft Attitude Control,” *Journal of Guidance, Control, and Dynamics*, Vol. 41, No. 9, 2018, pp. 1990–2001. <https://doi.org/10.2514/1.G002873>.
- [12] Ed. by Wertz, J. R., *Spacecraft Attitude Determination and Control*, Astrophysics and Space Science Library, Springer Netherlands, 1978. URL <https://books.google.com/books?id=crTwCAAAQBAJ>.
- [13] Kirk, D., Kirk, D., and Kreider, D., *Optimal Control Theory: An Introduction*, Networks series, Prentice-Hall, 1970. URL <https://books.google.com/books?id=8vVQAAAAMAAJ>.
- [14] Markley, L., and Crassidis, J., *Fundamentals of Spacecraft Attitude Determination and Control*, 2014. <https://doi.org/10.1007/978-1-4939-0802-8>.